Jasper Hendricks
Student number: 0423475
jasperhendricks@gmail.com
Bos en lommerweg 33-3
1055 DK Amsterdam

The option of phase change materials as temperature regulation for building integrated photovoltaics

July, 2010

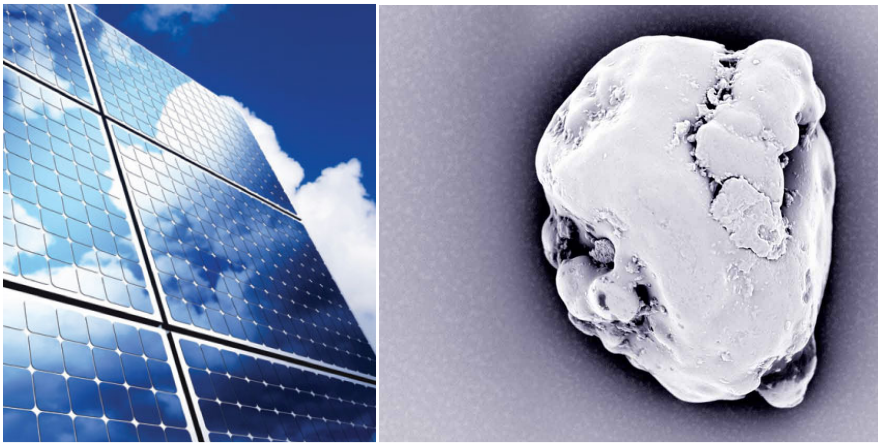

Report number: NWS-S-2010-18
Master Programme Sustainable Development; track Energy & Resources
Supervisor: Dr. W.G.J.H.M. van Sark
Department of Science, Technology and Society
Copernicus Institute, University of Utrecht, the Netherlands

Universiteit Utrecht

Abstract

The performance of photovoltaic modules outdoors suffers from attained high temperatures due to irradiation as a result of the negative temperature coefficient of their efficiency. Phase change materials (PCMs) are investigated as an option to regulate photovoltaic module temperature and thereby reduce its electrical efficiency decrease. Experimental set-ups have been studied by Huang et al. and Hasan et al. [1; 2; 3; 4], which showed significant improvements in the temperature regulation of building integrated photovoltaics (BIPV). In this study a simplified heat balance model is used to calculate the extra energy gain such a PV/PCM system can bring on a yearly basis. It is shown that on average an increase of 1-3% of the total energy output can be expected for several commercially available PCMs. However, when taking into account the PCM material cost this shows no economic potential for the future. For an acceptable payback period of 10-20 years the storage capacity of a PCM would require an increase in the range of one order of magnitude, which is not realistic. Further options might come from a combination with building climate control in which the PCM plays a double role controlling the PV temperature as well as the inside climate temperature.

Contents

1. Introduction

Solar insolation represents an abundant source of renewable energy. One way to use solar energy is the application of photovoltaic (PV) modules that transform the solar irradiation directly to electricity; other options are concentrated solar heating techniques that are connected to common turbine technology.
Photovoltaics have become a billion dollar industry but the costs (€/W) remain an important barrier in expansion of PV energy as a mainstream form of energy. Currently it is still four times too expensive to be commercially competitive with other common sources of energy [5]. It is therefore important to bring the cost down. This can be done by either lowering the production cost (e.g. thin film PV) or by enhancing the efficiency of the PV module in order to improve the €/W ratio.
The mainstream technique behind PV modules is based on single-junction solar cells based on silicon wafers, so-called first generation PV. For second generation PV, thin-film devices have been developed to cut the cost using less material and different active materials such as amorphous-Si. Most promising forms of PVs are classified as third generation PV and one of these is based on multi junction devices that have a much higher efficiency but should share the same costs as first or second generation PV, e.g. 32% efficient, thin-film GaInP/GaAs/Ge triple-junction PV. These technologies are appearing but still in an experimental phase and with too high costs [5]. It is expected that up until 2020 first and second generation PV will dominate the commercial PV sector and that by this time photovoltaics will have become a cost-competitive energy supply.
This thesis research is focused on building integrated photovoltaics (BIPV). This comprises photovoltaic modules that are directly integrated into the envelope of a building, serving a secondary purpose such as roof, façade or shading system.
BIPV makes up less than five percent in the current European PV market but has great potential due to high year-on-year growth and the increasing number of countries with supportive legislation. Crystalline silicon technology (especially mono-crystalline) is dominating the market with 90%, the other 10% is occupied by thin-film and other technologies. BIPV is applied in the residential sector as well as the public sector; the latter proves its importance as testing ground for new technologies and raising awareness [6].
Typical commercial silicon based cells convert only 10-20% of the incident light into electricity, the rest is transformed into heat, which causes a rise in temperature of the PV module [7]. Elevated operating temperatures are known to reduce the solar to electrical conversion efficiency by 0.4-0.5% K^{-1} [1]. These temperature related efficiency losses account for 7.6 % of the total conversion loss on a yearly basis, making temperature a significant factor to account for [8]. Consequently one of the options to enhance efficiency is to keep the temperature of the PV cell as low as possible, preferably at the operating level of the so-called standard test conditions (STC) of 25 ^{o}C. Especially in BIPV, where modules are integrated in the building envelope and no natural ventilation on the rear side of the panel is generally possible, a temperature control means may be most effective. For PV modules that are attached to a building after construction, so-called building-added PV [9], temperature effects are less severe. This means the temperature of BIPV is more inclined to rise to higher temperatures and making temperature regulation even more important.
There are several techniques known in limiting the temperature rise of BIPV. Heat can be dissipated in a passive way using the natural convection of air in a duct behind the PV module but this is limited by a low rate of heat removal and accumulation of dust. Other active techniques that can be applied are forced air-cooling, hydraulic cooling or heat pipes. These might require additional energy use as well as construction costs.

In this research phase change materials (PCMs) are studied as a possible option to regulate the temperature rise of BIPV, as suggested by Huang [1]. These materials share a large latent heat and thermal conductivity and can absorb large amounts of energy at their phase transition temperature. Examples of materials are hydrated salts and paraffin waxes [10]. PCMs can be combined in a PV/PCM system in which the excess heat of the PV panel is absorbed by the PCM, i.e. the PCM acts as a latent heat storage keeping the PV module temperature constant during the phase change, which postpones the increase in module temperature and thus increases its electrical efficiency.

There have been a few studies investigating the temperature development in an experimental PV/PCM system set-up. Research by Huang [1] on two candidate PCMs suggests the concept is worthy of further development. Using environmentally friendly PCMs such as Rubitherm RT-20 and fins to enhance conductivity it is possible to reach a 10 ^{o}C temperature reduction for 5 hours at 1000 W/m2 insolation

The final objective of this research is to make an estimate of the total gain in energy output a PV/PCM system can bring in a yearly period. The purpose is to see whether the energy gain resulting from the addition of a PCM is significant and if there is economic potential for such a combination. Therefore a simulation model has been made to calculate the energy gain using yearly insolation and ambient temperature data and properties of different commercially available PCMs.

2. Background Theory

2.1 *Photovoltaic effect*

The photovoltaic effect exploits materials with semi-conductor properties. In a semiconductor system the electron orbitals are grouped into two energy bands. The lower band is called the valence band and the upper band is called the conduction band. These two bands are separated by an energy gap E_g. Conductivity in a semiconductor arises from the presence of electrons in the conduction band or unoccupied orbitals in the valence band, which are so-called holes [11; 7]. These electrons and holes can either be created by thermal excitation/photon absorption that promotes electrons from the valence to the conduction band, or the presence of impurities that change the balance between the number of electrons and holes.
In a common single-crystalline solar cell the semi-conductor is silicon that gets doped in order to create impurities. This results in the so-called p-type material that has holes as majority carrier, and n-type material that has an excess of electrons as majority carriers.

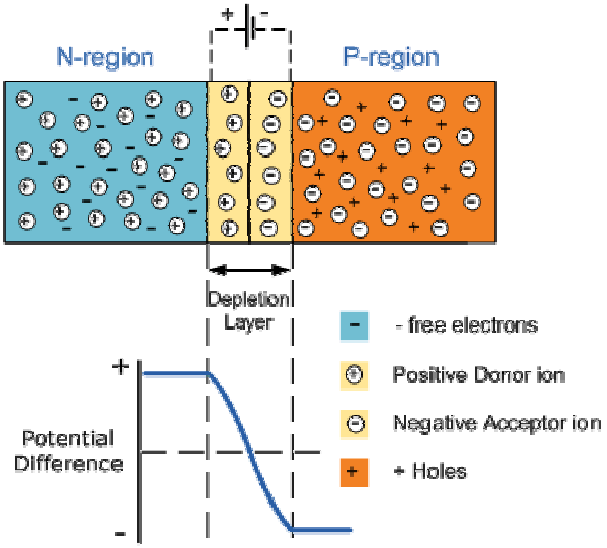

Fig.1. Potential difference between n- and p-type material.

Photon energy has to be equal or greater to the bandgap energy *Eg* in order to create a free electron and a corresponding positive charged hole.
In a p-n junction without illumination there are two currents generated. One is a small generation current I_0 called saturation current that is predominantly controlled by temperature. It is the exchange of the electron and hole minority carriers to their respective n- and p-type side of the junction. A recombination current flows in the opposite direction to restore the normal internal electric field. This current can be varied by a potential voltage difference.
It gives the following net current in a photovoltaic cell when there is no illumination, the so-called dark current:

$$I_d = I_r - I_0 = I_0(e^{eV_b/kT} - 1) \quad (1)$$

In which e is the elementary charge, V_b the electrical potential, k the Boltzmann constant and T the absolute temperature. When the photovoltaic cell is illuminated an absorption of photons takes place if

$$hv \geq E_g \tag{2}$$

where h is the Planck constant (6.63 * 10^{-34} J s^{-1}) and v is the radiation frequency. The bandgap in solar cell material is approx. 1.1 eV. The photon absorption creates electron-hole pairs, which are separated by the internal electric field that is caused by the p-n junction. This causes a dominating generation current of carriers induced by illumination which can be defined as:

$$I_L = eS(L_n + L_p) \cdot g_{op} \tag{3}$$

in which S is the p-n junction cross-sectional area, L_n and L_p the diffusion length for electrons and holes respectively, and g_{op} is the rate of optical carriers generation [12].
The total output current is the difference between the dark current and the light generated current, which gives us the following:

$$I_T = I_0(e^{eV_b/kT} - 1) - I_L \tag{4}$$

In fig.2 we see I_L and I_D plotted against voltage. It is clear that the highest power output, i.e. the highest efficiency is reached when there is a high short circuit current and a high open circuit voltage.

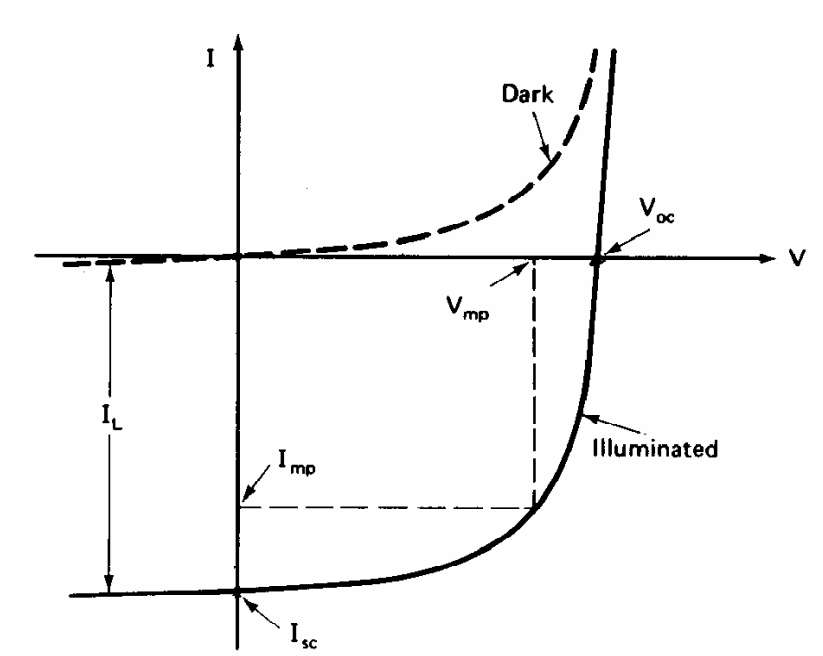

Fig.2. Plot of dark and light-generated current against voltage [13].

The maximum power (W_p) of the solar cell is thus given by:

$$P_{\max} = V_{mp} \cdot I_{mp} = ff \cdot V_{oc} \cdot I_{sc} \tag{5}$$

In which ff is the ratio that links the maximum power output to the theoretical output, the so-called fill factor. The efficiency of the cell is:

$$\eta = \frac{ff \cdot V_{oc} \cdot I_{sc}}{E \times A} = \frac{P_{\max}}{E_{in}} \tag{6}$$

in which E_{in} is the total irradiance ($W\ m^{-2}$) under STC conditions, and A is the total surface of the solar cell (m^2). Current efficiencies of wafer based silicon cells are in the range of 10-20%. This means there are a lot of conversion losses, most of which are intrinsic to the photovoltaic effect. Most energy is lost because the energy of the photons is outside the range of the bandgap energy, either to low or too high. This accounts for a total of around 50% loss [7]. The rest of the losses can be ascribed to voltage factor, collection efficiency of charges after carrier generation, I-V characteristic, etc.

2.2 *Photovoltaic effect and temperature*

Another important factor that causes an important loss of efficiency is the temperature of the module, which plays the major role in this research. According to Iliceto [8] this is 7.6% in crystalline silicon solar cells on a yearly basis. Temperature increase has several physical influences on the solar cell material:

- decrease of band gap,
- increase of thermal lattice vibrations,
- decrease of charge carriers density,
- reduction of the p-n junction voltage and its ability to separate photon induced electron-hole pairs.

The bandgap energy decrease (for silicon this is $-2.8*10^{-4}$ eV K^{-1}) means that more electrons can overcome the energy gap by thermal activation. The temperature dependence of I_{sc} is given by:

$$\frac{1}{I_{sc}} \frac{dI_{sc}}{dT} = 0.033\% / K \tag{7}$$

Other sources like Green [13] and van Dyck in [14] report 0.04-0.06%./K.
The additional creation of electron-hole pairs causes an increase in dark current, and consequently a decrease in open circuit voltage $V_{oc.}$
The voltage dependence on temperature is given in the following formulas [12]:

(8)

(9)

Using typical silicon solar cell values (T_0=300K, E_{g0}=1.21 eV and $V_{oc}(T_0)$=0.55V) a typical decrease of -2.45mV/K or 0.4%/K is found.

Since the increase in short circuit current is a factor 10 smaller this results in a net decrease of power output. This is visible in figure3 in which the power output is plotted against voltage for different temperatures. According to theory there is a linear decrease of 0.4%/K, whereas experimental values result in 0.65%/K. This value will be used in the model to calculate the power output difference between a reference system and a PV/PCM system.

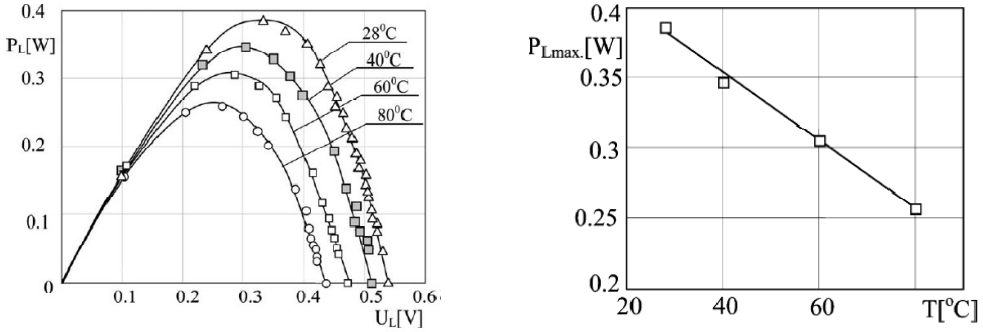

Fig.3. First graph shows the relation between power and voltage. Second graph shows the linear relation between power and temperature [15].

2.3 Phase Change Materials

Phase change materials have been investigated over the last 20 years as an efficient latent heat storage material [16]. Latent heat is the amount of heat that is absorbed or released during a phase transition of a material (e.g. solid to liquid or liquid to gas or vice versa) while the temperature of the material remains the same (isothermal process). The most common method used to store thermal energy is the sensible heat method, in which the heat is absorbed or removed by a change of temperature and without a phase transition. This is for example applied in solar heating systems in which water is used for heat storage in liquid systems and a rock bed is used for air-based systems.

Latent heat storage however has a much higher energy storage density during a smaller temperature change. Using phase change materials as latent heat storage makes it possible to store 5-14 times more heat per unit volume then sensible heat storage due to the phase change that occurs [17]. This can be seen in fig.4. Many applications of PCMs as latent heat storage have been investigated and are summarized in [16; 10; 17].

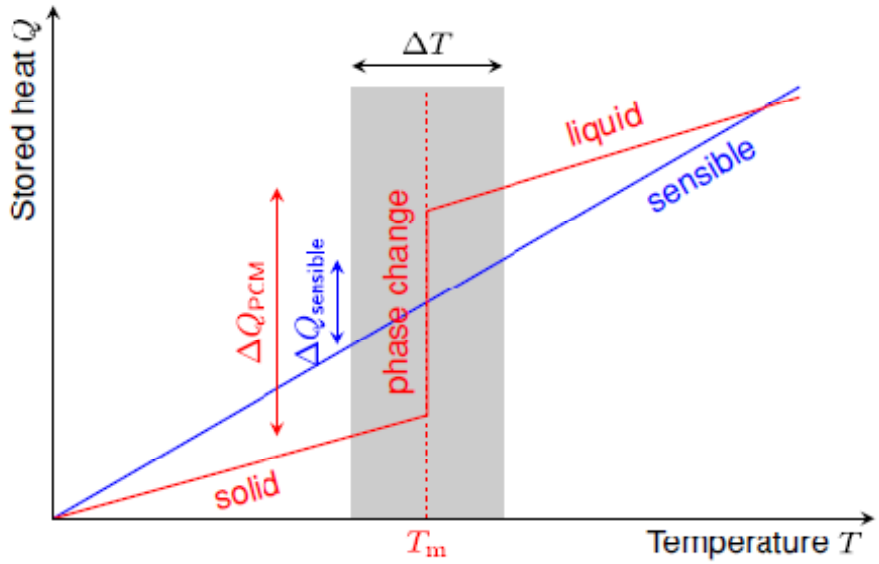

Fig.4. Phase change materials can store a large amount of heat during a small temperature interval [18].

A wide selection of PCMs is known with a heat of fusion in any required range, but a PCM requires several thermodynamic, kinetic and chemical properties in order to be applicable in the desired way. One can think of the following [17] [17]:

Thermal properties
- Suitable phase-change temperature
- High latent heat of fusion
- Good heat transfer/conductivity

Physical
- Favorable phase equilibrium
- High density
- Small volume change
- Low vapor pressure

Chemical
- Long-term chemical stability
- Non-toxic
- No fire hazard
- Non-corrosive

Economics/Environmental
- Cost effective
- Large-scale availability/abundance
- Environmentally sound/degradable.

The wide selection of PCMs can be classified on their raw material basis as follows (fig.5).

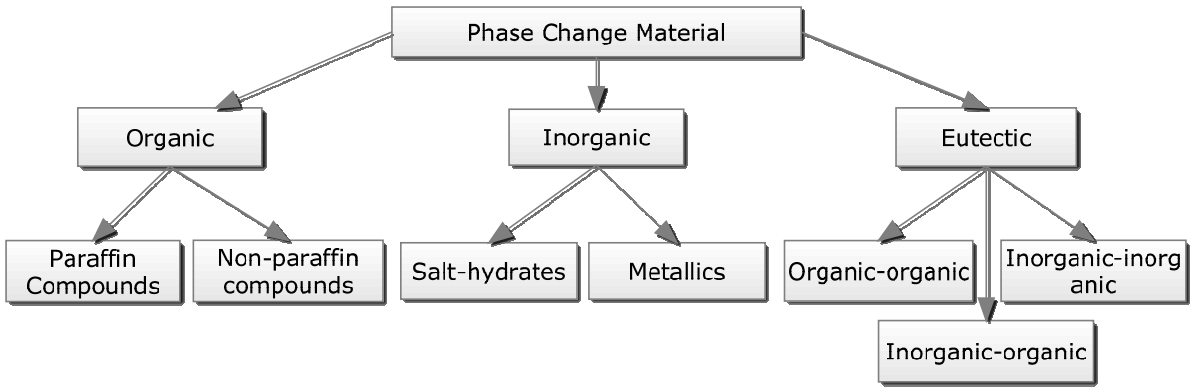

Fig.5. Classification of PCMs.

Organic paraffin wax consists of mostly straight chain n-alkanes CH_3-$(CH_2)_x$-CH_3 and is a safe and non-corrosive PCM. Their low conductivity and volume change however are two important drawbacks. Different paraffin waxes in particular share the same properties while the non-paraffin waxes have the most varied properties. One important subgroup are the so-called fatty acids which have high heat of fusion values compared to paraffins but the cost are 2-2.5 times higher than paraffins.

Inorganic PCMs can be made of salt hydrates or metallics. Salt hydrates have been the most important group of PCMs studied until now. They are made of inorganic salt and water and have the general formula $AB.nH_2O$. The most important characteristic is the higher latent thermal conductivity, which is almost double that of paraffins. Major drawback is the problem of incongruent melting which occurs when there is not enough water to dissolve all the salt and the solid residue is not available for recombination any longer.

Metallics have a high thermal conductivity but have not been seriously considered due to their high weight. Eutectics are formed by a mixture of two or more components that can be both organic and inorganic.

All PCMs share a common problem of generally low heat conductivity due to the crystallizing and thickening agents that are used to prevent supercooling and phase separation [19].

An overview of positive/negative features for each group is given in table 1.

Table1. Several positive/negative features of different PCM materials [16; 17].

PCM materials	*Positive features*	*Negative features*	*Promising examples*
Organic-paraffin	-available in large temperature range -safe, reliable, non-corrosive -excellent thermal stability	-low thermal conductivity -moderately flammable -volume change	-technical grade paraffins: 6106,P116,5838, etc. -Rubitherm RT-27.
Organic-non-paraffin (fatty acids)	-high latent heat of fusion	-low thermal conductivity -flammable -varying toxicity -2-2.5 higher cost than technical grade paraffin's	-D-Lattic acid, Cyanamide, Methyl behenate, Trimyristin, acetic acid, Myristic acid, Acetamide, etc..
Salt Hydrates	-high latent heat of	-slightly toxic	-$CaCl_2.10H_2O$, $LiNO_3.2H_2O$,

	fusion -higher thermal conductivity (double that of paraffins) -sufficiently inexpensive	-incongruent melting -corrosive	$FeCl_3.2H_2O$
Metallics	-high thermal conductivity	-low heat of fusion per unit weight	-Gallium, Cerrobend eutectic
Eutectics	-congruent melting	-dependent on mixture	-Triethylolethane+urea, $CH_3COONa.3H_2O+NH_2CONH_2$.

2.4 *Selection of PCMs*

The paper by Sharma [17] reviews an extensive number of PCM applications and it becomes clear that in most cases either paraffin waxes or salt hydrates are chosen as the best candidates, e.g. commonly used PCMs in building applications are salt hydrates and hydrocarbons.
Since low conductivity is a common factor in PCMs the two important factors for a selection become the melting temperature and the heat of fusion. Besides that the cost factor and its environmental impact features are important.
With this in mind there are several PCMs available at the moment that could be used in a PV/PCM system, most of which are commercially available (table 2).

Table 2. Several commercially available PCMs. The ones used in the model calculations are highlighted.

PCM[1]	*Raw material*	*Melting temperature* (^oC)	*Heat of fusion* ($kJ\ kg^{-1}$)	*Density* ($kg\ m^{-3}$)	*Heat conductivity* $W\ m^{-1}\ ^oC^{-1}$	Manufacturer
ClimSel 24	Salt hydrate	24	144	1480	0.5-0.7	Climator
STL47	Salt hydrate	47	221	1340		Mitsubishi Chemical
RT27	**Paraffin**	**27**	**184**	**880**	**0.2**	**Rubitherm GmbH**
RT42	**Paraffin**	**41**	**174**	**880**	**0.2**	**Rubitherm GmbH**
GR50	Paraffin	49	55	849	0.2	Rubitherm GmbH
Thermusol® HD35SE	**Salt hydrate**	**35**	**160**	**780**	***n.a.***	**Capzo International BV**

[1] PCM properties deducted from [41], [36], [42], [4].

Thermusol® HD60GE	Salt hydrate	55	200	780	*n.a*	Capzo International BV
DS 5001	**Paraffin**	**26**	**110**	**250-350**	***n.a.***	**BASF**
RT20	Paraffin	22-25	240.3	870	0.2	Rubitherm GmbH
Capric-lauric acid	Eutectic	21-24	172	880	0.14	*n.a.*
Capric-palmitic acid	Eutectic	22-26	196	880	0.14	*n.a.*
$CaCl_2.6H_2O$	Salt hydrate	29	213	1710	1.1	*n.a.*
SP22	Salt hydrate	23-24	182	1380	0.6	Rubitherm GmbH

The latter five PCMs in the table are used by Hasan et al [4]. Other Rubitherm PCMs that were used by Huang [1] are RT26 and GR40. The latter consists of a granulate PCM encapsulated by a background material in order to keep it in a permanent solid state and avoid liquid handling. Granular PCM are found to be less effective than RT because of the bulk thermal conductivity that is reduced by the air between the granules.
The phase change materials made by Rubitherm are based on paraffins and waxes. According to Rubitherm these products are non-toxic, ecologically harmless and 100% recyclable. More safety data can be found in the appendix B. It is clear that every PCM has some negative features but in this research the choice is made for organic paraffins because they are the best candidates for environmentally friendly PCMs. The low conductivity and volume change are serious shortcomings but progress is being made to overcome these issues.
Other commercial PCMs that are later used in model runs are the Thermusol HD35 fabricated by Capzo International and DS5001 by BASF. Both these PCMs are encapsulated so they keep their solid structure, which makes them easier to handle.

2.5 *Heat balance PV/PCM system*

The following section explains the idea of a PV/PCM system using a heat balance perspective. The PCM is attached to the PV module and will act as latent heat storage and absorb the excess heat that is generated in the PV module as a result of solar insolation. Figure 6 shows the external heat transfer present in an experimental PV/PCM system set-up.

The incident solar irradiance I_r on the PV cells acts as the supplier of energy (heat). This is dissipated by the heat loss coefficients on the front and rear side of the panel and absorbed by the PV cell and the connected PCM. It is assumed there is no heat loss from the top or bottom of the system.

This simplified energy balance is described in the

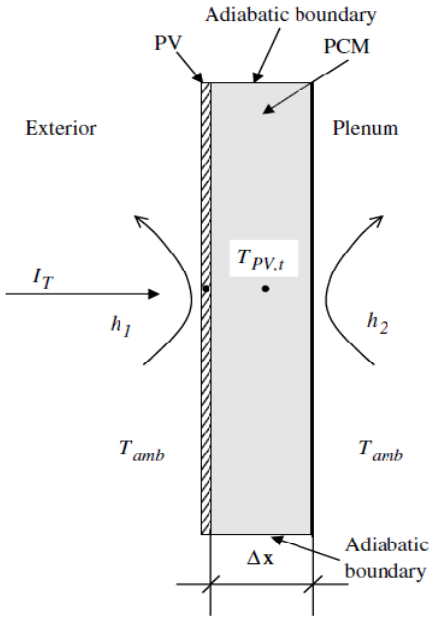

Fig.6 Experimental PV/PCM system set-up [2].

following formula [1]:

$$\Phi \cdot \Delta t \cdot (\alpha - \eta_{pv}) = U_L \cdot \Delta t \cdot (T_{PV} - T_{amb}) + Q_s \tag{10}$$

The total irradiation Φ is corrected for the part that is actually contributing to the heat balance, so the part that is transformed into electricity (represented by the module efficiency η_{pv}) is subtracted and there is an absorbance factor α taken into account. The total heat loss coefficient U_L describes the heat that is dissipated from the system during time-step Δt . Qs represents the heat absorbed by the PCM at the back of the PV. This is described in three different stages because of the phase transition of the PCM where T_m is the melting temperature of the PCM. It is assumed that the specific heat difference of the PCM in liquid and solid phase is negligible [4].

$$\begin{aligned} Q_s &= mc(T_{PV} - T_{amb}), && T_{amb} < T_{PV} < T_m \\ Q_s &= mc(T_m - T_{amb}) + H, && T_m \le T_{PV} < T_m + \Delta T \\ Q_s &= mc(T_m - T_{amb}) + H + mc(T_{PV} - T_m), && T_{PV} \ge T_m + \Delta T \end{aligned} \tag{11}$$

The three equations reflect the three different states of the PV/PCM system in which H stands for the latent heat of fusion, i.e. the heat storage capacity of the PCM. In the first stage the temperature of the PV is below the melting temperature of the PCM, which means it has been absorbing heat as sensible heat storage. If the PV system temperature reaches the melting temperature of the PCM it starts to act as latent heat storage and absorbs a large amount of heat, melting in the process. This requires a certain amount of time and temperature until the total PCM is melted and cannot function as a heat sink anymore. At that point the temperature of the system will rise above the melting temperature and reach the same temperature as the reference system. The amount of heat that is stored is dependent on the specific heat, the temperature change and the amount of PCM material.

3. Methods/Model

The idea of the model is based on the heat balance described in section 2.5 and compares the temperature evolutions of a reference PV system and a PV/PCM system. A good representation of this idea is shown in figure 7 where the temperature evolution of the PV/PCM systems gradually increases to the PV reference temperature due to heat absorption by the PCM slab. The surface area between the two temperatures represents the thermal regulation enhancement, the temperature reduction gained by applying PCM. This difference will be used to calculate the extra energy output of the PV module by using an empirical relation.

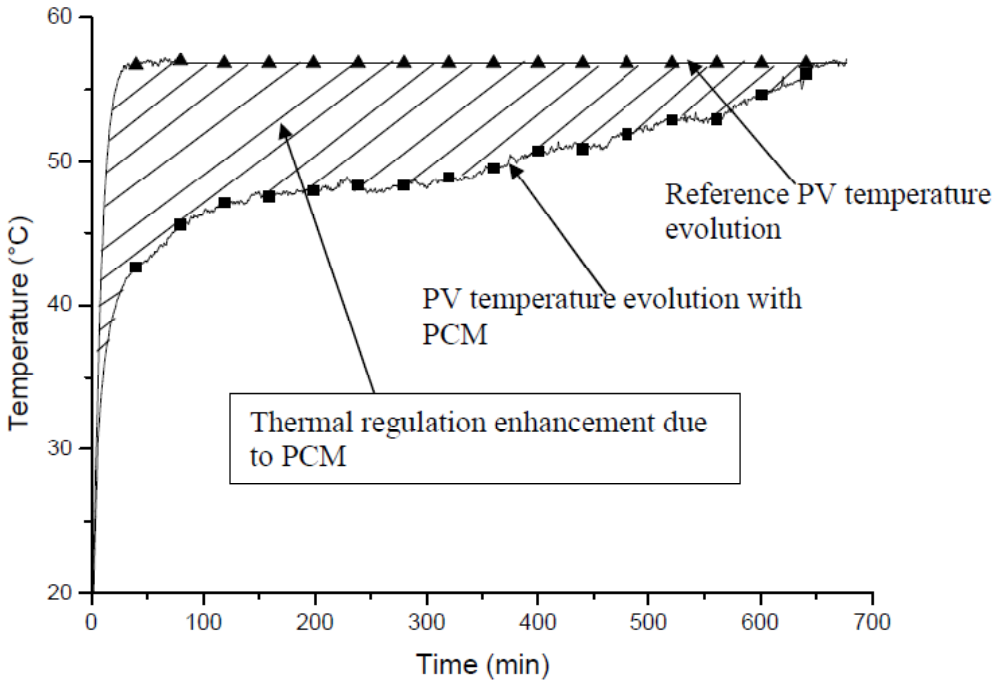

Fig.7. Temperature evolutions for PV reference and PV/PCM system [4].

3.1 *Reference system*

The reference PV system used is largely based upon the temperature model developed by Jones & Underwood [20] and a BIPV-Thermal model by Anderson et al. [21]. The module temperature is dependent on a range of variables like module material and weather conditions and the surrounding environment. A simple representation of this model is shown below. Because the calculations are done for a unit surface of 1 m^2 there is no surface variable present in the formulas.

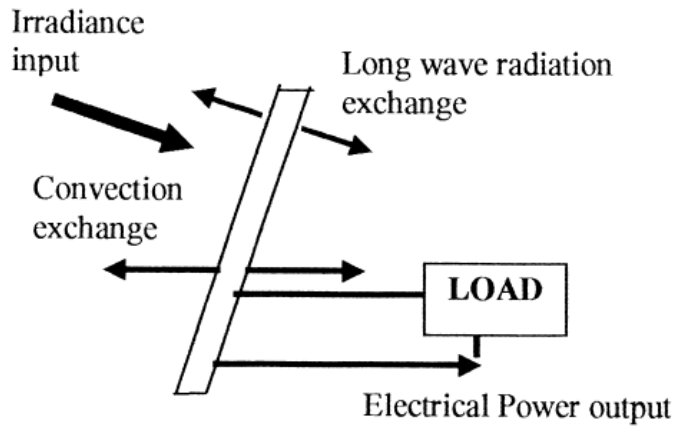

Fig.8. Different energy transfers in a reference PV system [20].

The scheme in figure 8 can be represented in the following way:

$$C_{pv}\frac{dT_{pv}}{dt} = Irradiance + Radiation - Power - Convection \tag{12}$$

in which the different energy in and outputs are equal to the temperature change and the specific heat capacity (C_{pv}). T_{pv} stands for the module temperature. The irradiance accounts for the total input of solar insolation and is defined as:

$$Irradiance = \Phi \cdot \alpha \tag{13}$$

where Φ represents the total solar energy input (W) and α is an absorptivity constant included to take only the absorbed insolation into account, i.e. part of the solar irradiation is reflected back and is therefore not part of the energy balance of the PV module.
Radiation stands for the net radiative heat transfer of the module and can be expressed in the following way:

$$Radiation = \sigma\varepsilon_p(T_{pv}{}^2 + T_s^2)(T_{pv} + T_s) \tag{14}$$

This is based on the Stefan-Boltzmann law, which states the relation between temperature and radiation. The emissivity of the module ε_p is included since the module is not a black body hence its emissivity is not 100%.
T_s is defined as the sky temperature using a modified Swinbank equation [21]:

$$T_s = 0.037536T_{amb}{}^{1.5} + 0.32T_{amb} \tag{15}$$

Third term of the balance is the power output of the module. This is an energy output dependent on the insolation and temperature of the module and described in the following way by [20]:

$$Power = C_{FF} \cdot \frac{\Phi \ln(k_1\Phi)}{T_{pv}} \tag{16}$$

in which C_{FF} is a fill factor model constant (1.22 K m^2) as well as k_1 (10^6 m W^{-1}). The heat loss caused by convection can be defined as:

$$Convection = (h_{front,natural} + h_{front.forced} + h_{rear}) \cdot (T_{pv} - T_{amb}) \tag{17}$$

Where the heat loss coefficients are split in a natural convection coefficient used for the rear side of the panel and a front panel coefficient. The latter exists of a forced component by wind and a natural component induced by the temperature difference. These are calculated in the following way [21]:

$$\begin{aligned} h_{front,forced} &= 2.8 + 3.0v \\ h_{front,natural} &= 1.78(T_{pv} - T_{amb})^{1/3} \\ h_{front,total} &= (h^3{}_{forced} + h^3{}_{nat})^{1/3} \\ h_{rear} &= 1.31(T_{pv} - T_{amb})^{1/3} \end{aligned} \tag{18}$$

The focus of the research is on BIPV systems, which means the rear side of the solar panel will be mounted in a building and it is assumed there will be no convection loss there [22]. A comparison will be made between normal PV systems and BIPV by either including the rear heat loss coefficient or leaving it out.
Combining the equations for the different parts gives the following expression for the rate of temperature change:

$$\frac{dT_{pv}}{dt} = \frac{\Phi \cdot \alpha + \sigma\varepsilon_p ({T_{pv}}^2 + T_s^2)(T_{pv} + T_s) - C_{FF} \cdot \frac{\Phi \ln(k_1 \Phi)}{T_{pv}} - (h_{front,natural} + h_{front,forced} + h_{rear}) \cdot (T_{pv} - T_{amb})}{C_{pv}} \tag{19}$$

3.2 *PV/PCM system*

Modeling of PCM temperature has been investigated thoroughly for the last 15 years but remains a challenging task. A 3-D PCM thermal control model has been developed by Huang et al [3], which uses computational fluid dynamics in order to predict the PCM temperature inside a small container which is dependent on a.o. the viscosity of the fluid and the movement of the solid-liquid boundary. Lamberg et al. [23; 24] have established an analytical and numerical solution for melting in a semi-infinite PCM storage using a heat equation for solid-liquid interface that is based on a 1-phase Stefan problem.
To calculate the temperature difference between a reference and a PV/PCM system it is necessary to add a component to the reference system equation that accounts especially for the heat storage by the PCM. In the simplified energy balance showed before this is represented by the latent heat of the PCM in the total time period of melting.
In the numerical approach this is done by including the heat conduction that occurs from the PV panel to the PCM. One-dimensional heat conduction can be represented in the following way:

$$\frac{\Delta Q}{\Delta t} = -k\frac{\Delta T}{\Delta x} \tag{20}$$

which shows that the change of heat Q over time is dependent on a heat conductivity parameter k and the temperature difference over a certain distance x .
Combining this with the latent heat storage the following expressions are used for the conduction part, as above, for three temperature-dependent states:

$$Conduction1 = k \cdot x \cdot (T_{pv} - T_{amb}) \qquad T_{amb} < T_{PV} < T_m$$

$$Conduction2 = k \cdot x \cdot H \cdot (T_{pv} - T_m) \qquad T_m \le T_{PV}, \sum_{i=0}^{n} k \cdot H \cdot S \cdot (T_{pv} - T_m) \le H \cdot m$$

$$Conduction3 = k \cdot x \cdot (T_{pv} - T_{amb}) \qquad \sum_{i=0}^{n} k \cdot H \cdot S \cdot (T_{pv} - T_m) \ge H \cdot m \tag{21}$$

The temperature difference between the front and the rear side of the system is chosen as the difference between ambient and module temperature when the PCM is not acting as heat storage. When the melting temperature is reached this difference is between melting and system temperature and the latent heat is included. When the temperature is above the melting temperature the heat stored in the PCM is summed over the total of time steps and it is verified if the summation has reached the total heat storage capacity of *H*m*, with *m* the total mass of the PCM material.

When modeling the phase change this latent heat must ideally be modeled as a continuous and invertible function of temperature (*h(T)*) since there is a phase change region, illustrated in figure 9.

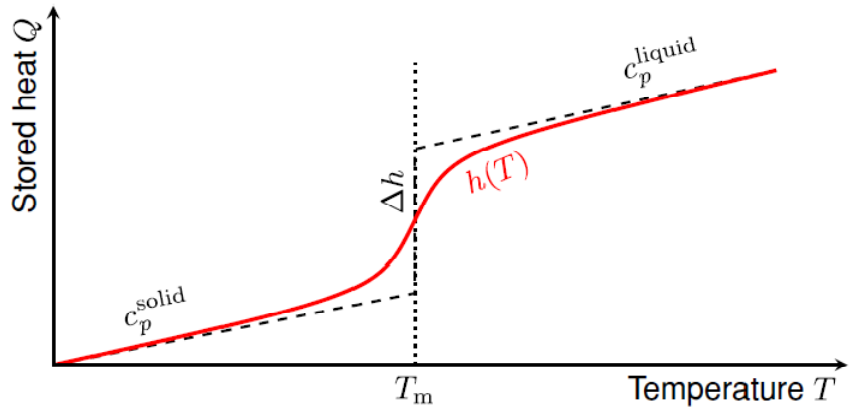

Fig.9. Representation of the storage capacity of an ideal PCM (dashed) and a real PCM (solid). In reality most PCMs show a phase change region instead of a melting temperature, best represented by an enthalpy function h(T) [18].

A numerical method to describe the PCM temperature is the enthalpy method, which is based on tracking the enthalpy (latent heat) change at the solid-liquid interface. Lamberg [19] describes an enthalpy form of the energy equation:

$$\rho \frac{\partial H}{\partial t} + h_c \nabla T = \nabla (k \nabla T) \tag{22}$$

where ρ represents density and the coefficient h_c is

$$h_c = 0.072 \left[\frac{\left[g((T_w - T_m)/2) \rho_l^2 c_{pl} k_l^2 \beta \right]}{\mu} \right]^{1/3} \tag{23}$$

With g the gravity acceleration constant (m s^{-2}), T_w wall temperature, β the thermal expansion coefficient (K^{-1}) and μ the dynamic viscosity (kg m^{-1} s^{-1}). The abbreviation l depicts the parameters in liquid state.
These equations can be solved using finite difference solution methods in order to calculate the enthalpy function $h(T)$ that has to be integrated into the PV/PCM temperature calculation. However, the calculation of $h(T)$ is dependent on the temperature that is calculated with the enthalpy function.
Besides this the higher mathematical approach is beyond the scope of the research and will increase the already high calculation times ($5*10^6$ time steps for yearly runs). These are the reasons that the latent heat is a constant in the equation and not temperature dependent. Instead an extra parameter S is added to the heat absorption equation that accounts for a simple diffusion of the heat uptake for every time step. The value for this parameter is chosen somewhat arbitrarily but is based upon the experimental results of Huang and Hasan et al. [1; 4].
The total expression now becomes:

$$\frac{dT_{PV}}{dt} = \frac{\Phi \cdot \alpha + \sigma \varepsilon_p (T_{pv}^{\ 2} + T_s^{\ 2})(T_{pv} + T_s) - C_{FF} \cdot \frac{\Phi \ln(k_1 \Phi)}{T_{PV}} - h_{total} \cdot (T_{PV} - T_{amb})}{C_{PV}} - \frac{Conduction}{C_{PCM}} \tag{24}$$

The Euler method is taken as numerical method to calculate T_{pv} for every time step. This method takes on the general form of:

(25)

in which the temperature of the panel at time step i is updated with the temperature change. The Euler numerical method is a first order approximation and thus less accurate for small time steps. It can become unstable with stiff equations especially using larger time steps. This concerns the model since we will be using time steps of 60 seconds. There are several other numerical methods to solve differential equations and it would be preferred to use an implicit method such as Runge-Kutta method. This however again increases the model run time and this level of accuracy is not relevant for the purpose of the study.

Figure 10 shows the temperature evolutions when using these expressions for two different insolation values.

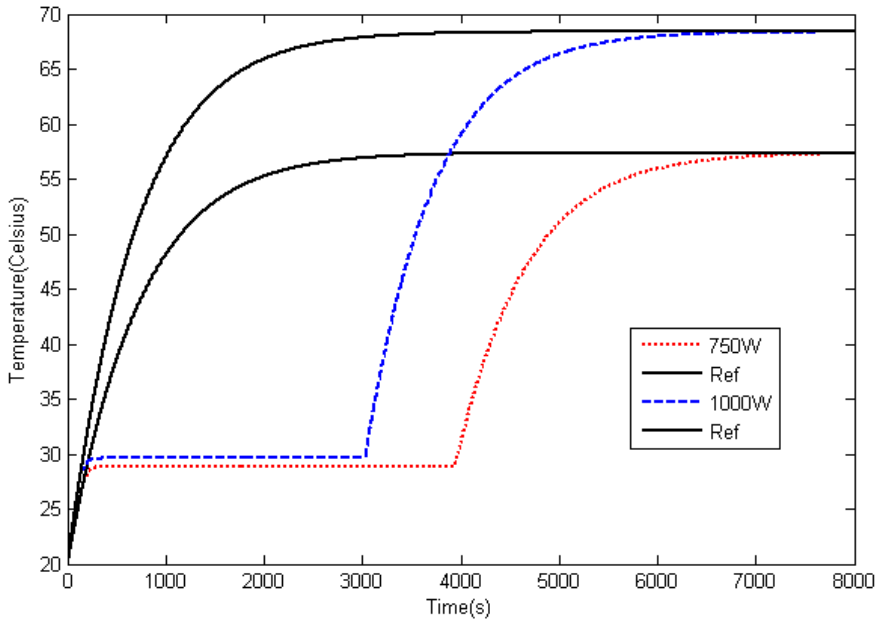

Fig. 10. Temperature evolutions for both reference and PCM system under different constant irradiation.

When the melting temperature is reached the conduction including the latent heat is activated (second stage) and keeps the temperature on a steady level until the total heat storage of the PCM is reached and the temperature resumes its normal curve.
In figure 11 we see two temperature evolutions from different authors that show the modeled temperature in the middle of a PCM slab. These both show the same 3-step curve shape as in the simplified model which supports the approach that is used.

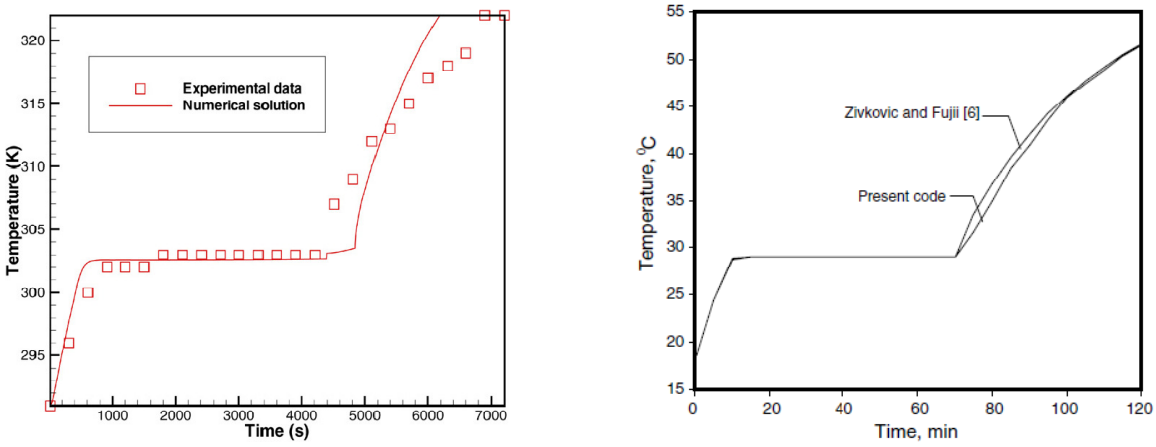

Fig.11. Two different temperature evolutions of the middle of a PCM container that show similar curve shape to the simplified code used. Wang [25](left) and Vyshak [26] (right).

3.3 *Energy output gain*

The simulated temperature difference between the reference system and the PV/PCM is used to calculate the difference in energy output at every time step. This is done with an empirical relation that uses a given percentage of decreased power K^{-1}. This percentage is experimentally set at 0.65% for a silicon type cell [15] and can be varied for other types of PV cells.
This results in the following expressions for energy output for each time step *n*:

$$E_{ref,n} = \eta \cdot \alpha \cdot \Phi_n \cdot \Delta t \tag{26}$$

$$E_{pcm,n} = E_{ref,n}[1 + d(T_{ref,n} - T_{pv,n})] \tag{27}$$

where E_{ref} stands for the reference energy output which is the starting point for the increase in energy output due to the PCM that is shown in (27). This relation assumes that the efficiency of the PV cells will increase with temperature decrease using the reference efficiency as a starting point, *d* being the increase in $J\ K^{-1}$ in percentage. To calculate the total energy enhancement during a period we can sum the difference over the total number of time steps and get:

$$E_{gain} = \sum_{n=0}^{n=t} (E_{pcm,n} - E_{ref,n}) \tag{28}$$

That gives the total energy output gain due to the PCM.

3.4 *Model Assumptions*

The major assumptions in the model are related to the PCM heat storage. The conduction term does not account for buoyancy and convective flows of the PCM melt. The actual yield is strongly related to the parameter *S,* which plays a major role in assigning the total heat storage of the PCM. The important drawback of this approach is the partly incorrect response on density and specific heat of the PCM due to the simplified formulation of the heat storage boundary. This is inconvenient but not limiting the results since the heat coefficient *S* combines the effect of these parameters and thus plays the major role in assigning the total storage capacity of the PCM.
Another interesting parameter is the heat conductivity *k* since it plays a role in the speed of the heat uptake by the PCM. In reality the conductivity of paraffin waxes is low but it is clear from the results that the temperature remains constant closely after the melting temperature has been reached. This reflects a scenario in which the conductivity is already strongly increased due to e.g. the addition of aluminum fins. The important thing concerning the conductivity and relevant for the model runs is that the heat storage limit is reached during the day period so the total latent heat of the PCM is optimally exploited.
Besides these two assumptions there are several other more common model assumptions worth mentioning. First of all only the heat transfer from the front and rear side of the panel are taken into account. The PV panel is assumed to be a thin layer of glass density with no extra layers such as cover material or backsheet.

Also a uniform wind speed is assumed. This means the convection loss coefficient due to wind is constant during the year, which has its influence on the temperature at a given insolation (e.g. if there is no wind during the day).
The volume expansion of the paraffin PCM is not considered. This can be up to 16% but is more relevant for the design of the system than the temperature evolution. There might be a small negative effect on the PV if the PCM releases its heat back to the PV when temperatures decline at the end of the day. This concerns PCM melting temperatures above operating temperature but is not included in the model because it is likely not significant.
There is a sensitivity analysis included in the results section to assess the significance of these assumptions.

4. Results

The PV/PCM model is used to make estimates about the energy output gain that results from the addition of the PCM to the back of the PV module. Input is in the form of insolation and ambient temperature data for the cities Utrecht (the Netherlands) and Malaga (Spain) [27]. This is hourly data (figure 12), which was interpolated into smaller time steps of 10s for day model runs and 60s for yearly runs. Table 3 contains the parameters for both PV panel and PCM properties that are used in the standard model runs. The calculations are performed using Mathworks Matlab 2009a. All results are calculated for an area of 1 m^2 panel.

Table 3. Standard parameters used in model runs.

Parameters	Symbol	Values
PV panel		
Absorbance factor[2]	α	0.95
Efficiency	η	0.15
Mass PV panel (glass) (kg m^{-2})	m	25
Specific heat PV panel (glass) (J kg^{-1} K^{-1})	c_{pv}	500
Power decrease K^{-1}	d	0.0065
Stefan-Boltzmann constant	σ	5.67 *10^{-8}
Emissivity sky[3]	ε_s	0.95
Emissivity module	ε_m	0.90
Average windspeed Malaga (m s^{-2})	υ_m	2.0
Average windspeed Utrecht (m s^{-2})	υ_u	3.3
PCM (RT-27)		
Thickness (m)	x	0.04
Heat absorbed factor	S	0.04
Conductivity (W m^{-1} K^{-1})	k	0.2
Melt temperature (K)	T_m	300
Specific heat ((J kg^{-1} K^{-1})	c_{pcm}	2000
Latent heat (J kg^{-1})	H	184000
Density (kg m^{-3})	ρ	880

Together with the insolation data these properties form the total input of the model. Figures 12-13 show both the daily average insolation and daily average energy gain. Figure 14 combines these energy gain and insolation values and shows that Malaga on average has a higher energy gain per day which is mainly due to its higher insolation values. It is also clear that Utrecht has a lower energy gain at some points while the average insolation values are the same. This can be ascribed to the difference in temperature evolution and insolation during the day (figures 15-17) since the energy gain is dependent not only on the temperature difference, but also on the value of insolation at a given moment.

[2]Value taken from [31],
[3] Emissivity values taken from [20].

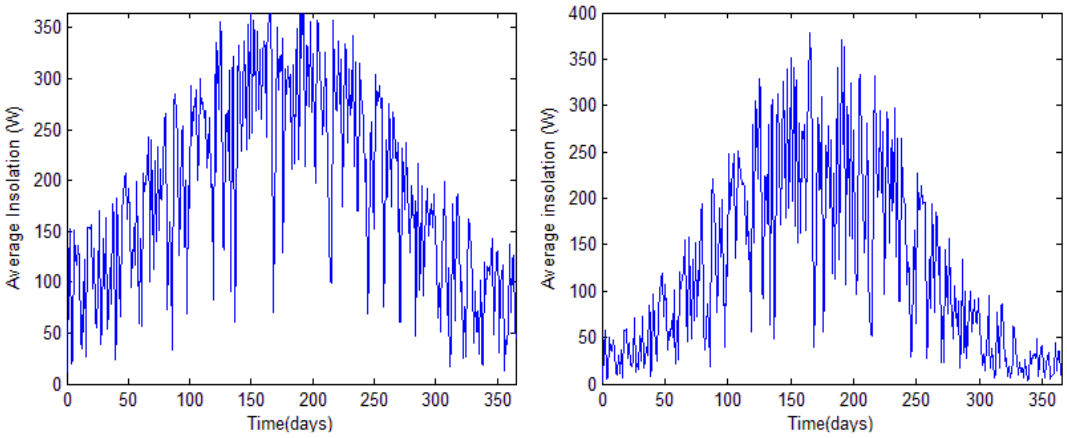

Fig.12. Daily average insolation for Malaga and Utrecht respectively.

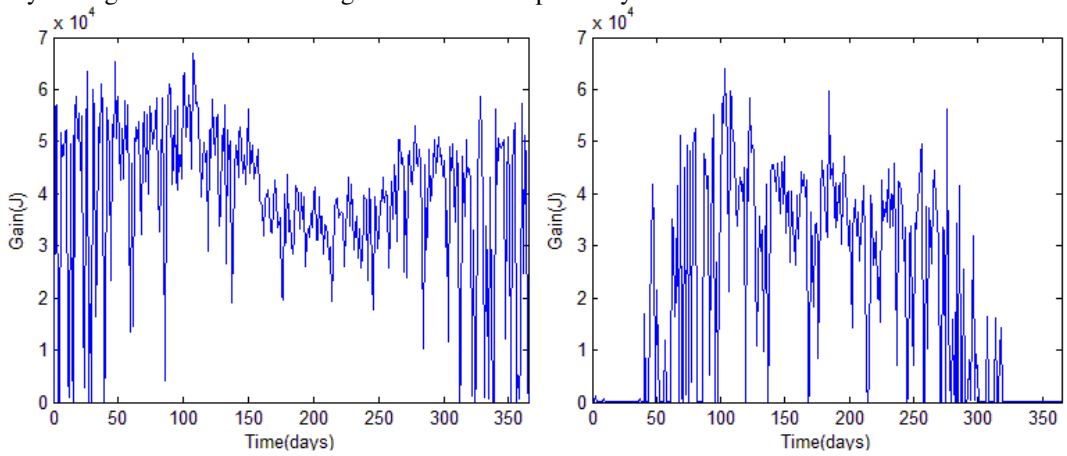

Fig.13. Daily average energy gain for Malaga and Utrecht respectively.

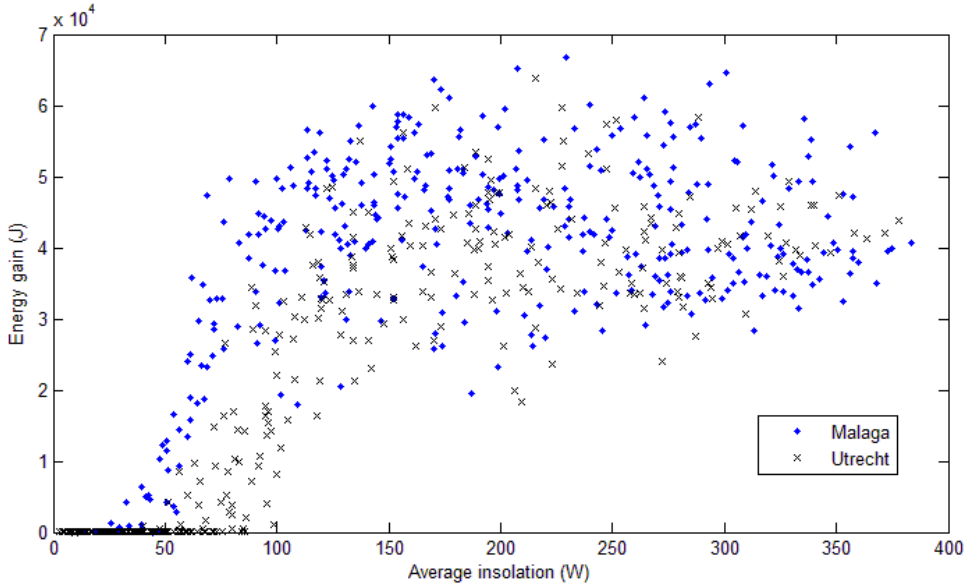

Fig.14. Daily average insolation values versus daily average energy gain for both Malaga and Utrecht.

Figures 15-17 show an idea of the amount of PCM enhancement that can be expected during a daily period. Values for energy gain are given in parenthesis.

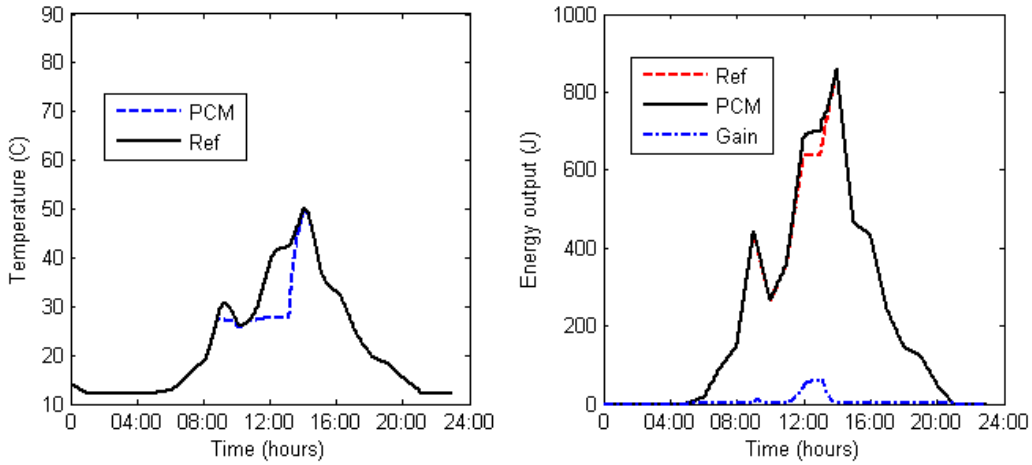

Fig.15. Reference and PCM temperature evolutions and energy output for Utrecht 24apr with BIPV and RT-27 ($4.01*10^4$ J).

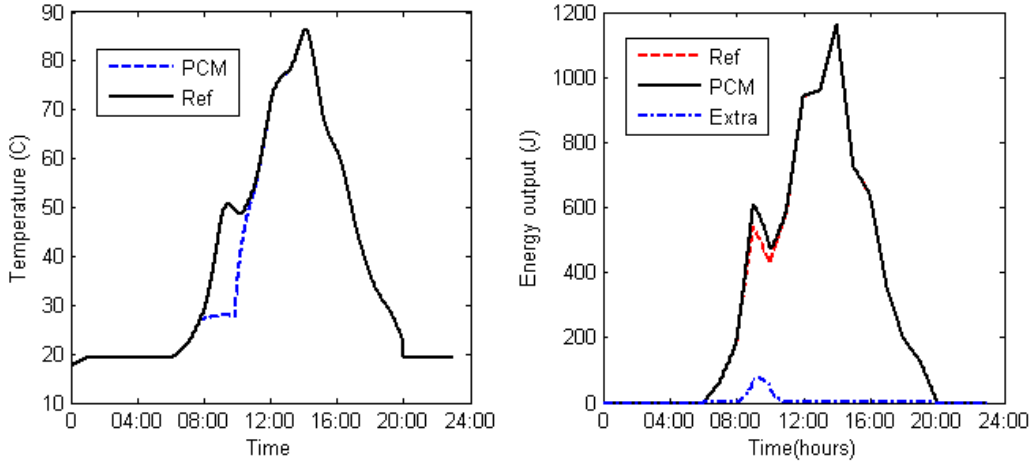

Fig.16. Reference and PCM temperature evolution and energy output for Malaga 24apr with BIPV and RT-27 ($3.97*10^4$ J).

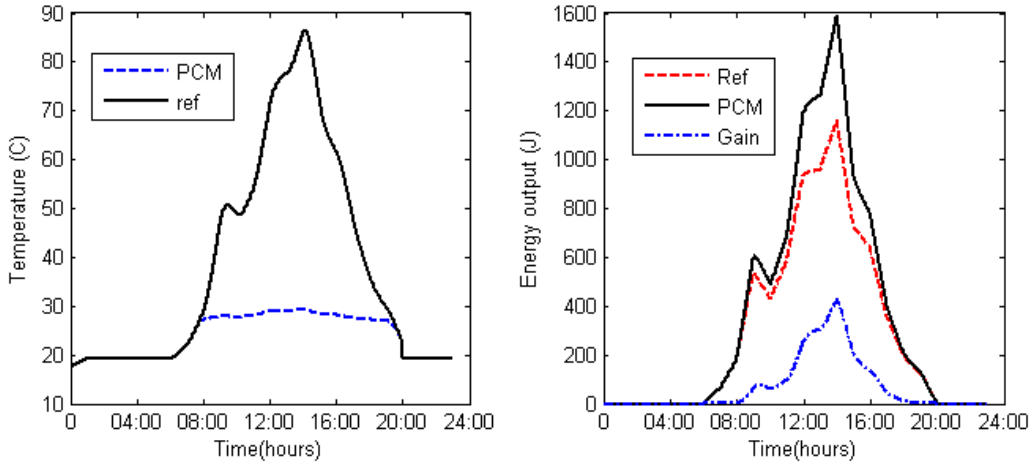

Fig.17. Reference and PCM temperature evolutions with maximum latent heat storage using S = 0.0004 ($5.77*10^5$ J).

Figures 15-16 show that the temperature is kept almost constant for a ~2-4 hour period after which the heat storage capacity is reached and the temperature starts to follow the reference model. For Malaga the temperature reaches a maximum of 86 degrees, a high temperature caused by the absence of rear panel convection. Figure 17 represents a scenario in which the

total heat storage has no limit and the temperature can be controlled during the whole day. This theoretical maximum is an interesting scenario for payback period calculations.

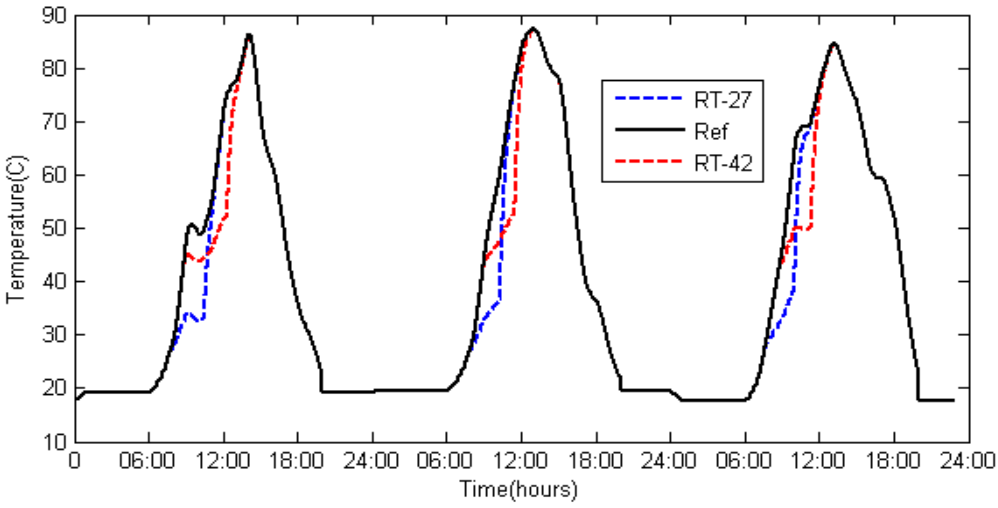

Fig.18. Temperature evolutions on 24/25/26 April Malaga for both RT-27 ($1.37*10^5$ J) and RT-42 ($2.11*10^5$ J).

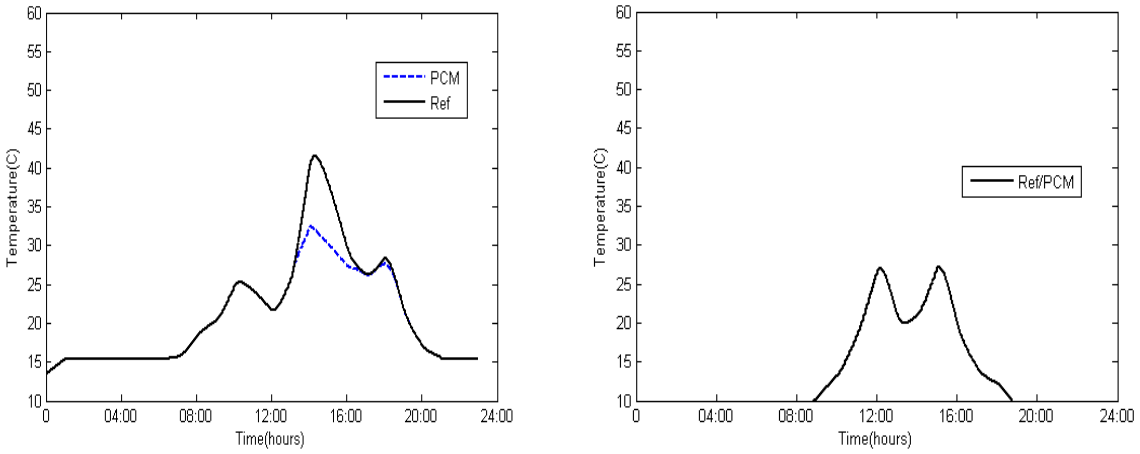

Fig.19. Temperature evolutions for Utrecht on 24 Aug. ($2.84*10^4$ J) and 24 Feb. (76 J) respectively. On Feb. 24 the melting temperature is not reached and there is almost no gain caused by the PCM.

Figures 18-19 above depict the importance of the melting temperature. This temperature is important since it defines the moment when the PCM starts taking up heat. Figure 18 shows a 3 day period temperature evolution for 2 PCMs with different melting temperatures. It is clear that both PCMs are activated at a different time. The area that represents the total heat stored stays the same so the energy gain is expected to be the same as well for both PCMs. However, when the temperature is controlled at a higher insolation (i.e. higher temperature) this causes an increased reference energy output and this results in a higher corresponding energy gain (see formulas 26, 27).

When the PCM melt temperature is higher using RT-42 we see only a small difference in yearly power output where one would have expected less output since the temperature does not reach above 40 degrees for a considerable period of the year. This is again due to the moment the PCM starts taking up heat, with a higher melt temperature the PCM acts at higher insolation values which cause a higher reference energy output. It is actually only the temperature difference that is important since the relation between energy decrease and temperature increase is a linear one.

This shows the importance of the choice of melting temperature in relation to the yearly insolation values. This is also shown in figure 19 where a melting temperature has to be below 40 degrees to be effective. There are also days in the year where the PV temperature does not rise above the PCM melting temperature and it does not have any influence and a lower melt temperature would be preferred. This makes areas with more insolation and building integrated PV a better option since the temperature rises above a higher melting temperature more often.

4.1 *'Sensitivity analysis '*

The following section contains an analysis on the influence of the important parameters on the results. The PCM characteristics are varied but not in a percentual way. Results are depicted in table 4. The annual gain in Utrecht is lower which is expected since the insolation is lower than in Malaga due to weather conditions and latitude. A percentage of the total energy output is included to give a better comparison. Besides the PCM characteristics in table 4 the efficiency, heat absorbance factor (*S*) and wind speed are varied by -10% and +10%, results are shown in figure 22.

Table 4. Energy gain for different PCM characteristics. Percentage calculated on a total of 227 and 150 kWh for Malaga and Utrecht respectively.

	Melting temperature (K)		Latent heat (kJ kg^{-1})			Thickness PCM (m)			S (-)		
Range	27	42	100	184	268	0.02	0.04	0.06	0.02	0.04	0.06
Malaga											
($J*10^6$)	12.7	18.1	7.58	12.7	21.7	6.7	12.7	24.5	34.1	12.7	9.42
(kWh)	3.53	5.03	2.11	3.53	6.03	1.86	3.53	6.81	9.47	3.53	2.62
(%)	1.55	2.22	0.93	1.55	2.66	0.82	1.55	3.00	4.17	1.55	1.15
Utrecht											
($J*10^6$)	7.37	6.78	4.35	7.37	10.4	3.56	7.37	11.2	15.1	7.37	4.82
(kWh)	2.05	1.88	1.21	2.05	2.89	0.99	2.05	3.11	4.19	2.05	1.34
(%)	1.36	1.26	0.81	1.36	1.92	0.66	1.36	2.10	2.79	1.36	0.89

It is clear from the energy gain that Malaga has the greatest potential for a PV/PCM system, which is due to the weather conditions and the total energy output. From a percentual view the standard run stays in the same range of ~1.5%. There is a significant increase using a higher melting temperature in Malaga. The energy gain stays in the range of 1-3% with a serious increase in latent heat and PCM thickness. Figure 20 and 21 show two examples of daily temperature evolutions with changing parameters of PCM thickness and *S* respectively. It is clear that both parameters have an important influence on the total energy gain. The relation between thickness and the total heat stored during the day is a more linear relation than with the S values.

The analysis in figure 22 shows the linear relation between reference PV efficiency and energy gain. The energy gain stays between 3 and 4 kWh on a total reference output of 227 kWh yr^{-1}. The figure also shows that the most important parameter *S*, which is responsible for the amount of heat storage capacity has a mild exponential relation and no exceptional gain is expected with larger decrease. The amount stays between 1-2% of the total energy gains.

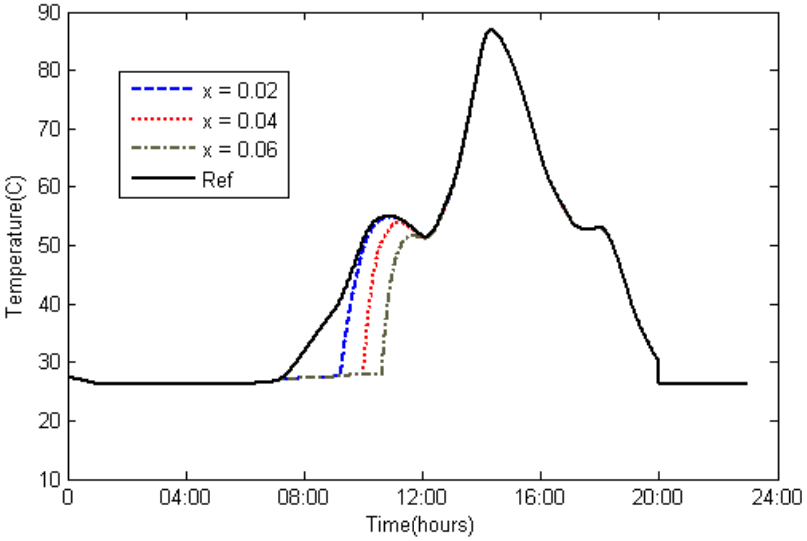

Fig.20. Temperature evolution for 24 Aug Malaga with different PCM thickness.

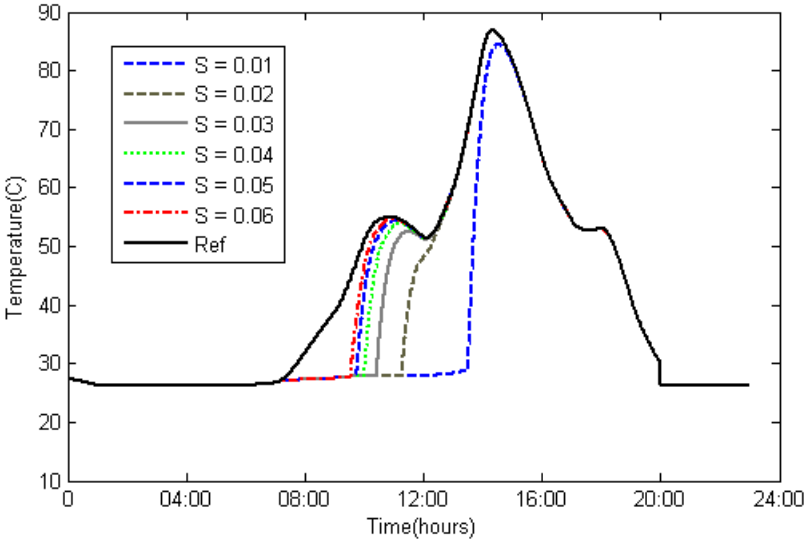

Fig. 21. Temperature evolution for 24 Aug Malaga with different S values. It is clear there is no linear relation between S and the total capacity of heat storage.

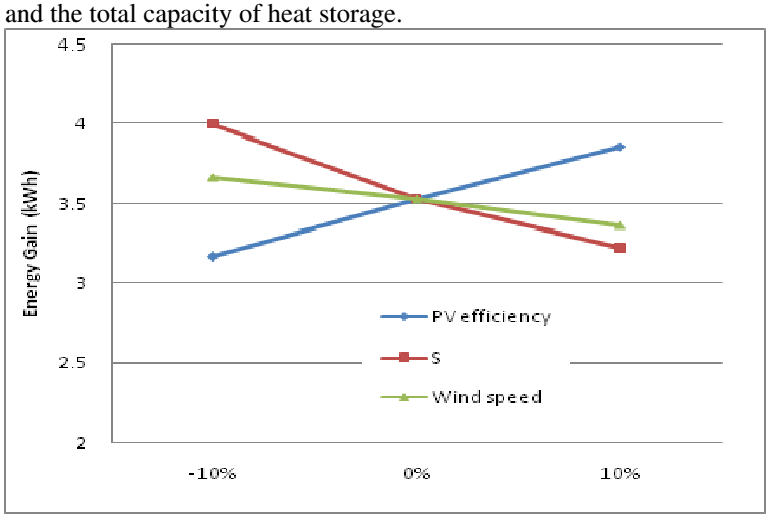

Fig.22. Sensitivity analysis for 3 different model parameters.

4.2 *Building-added PV*

Although this research was focused on BIPV some model runs are carried out to see whether there is a difference between the application of PCM in building integrated or building-added PV; results are shown in Table 5.
For the BIPV results it is assumed there is no convective heat transfer from the back of the module, which causes the temperature to rise to a higher level. The energy gain is slightly higher for BIPV. This is likely due to the higher temperature of the system over the whole year period, which enables the PCM to act as latent heat storage more often.
The difference is also dependent on the melting temperature, i.e. with higher melt temperature the PCM gets more opportunity in the BIPV scenario. This is shown by the increase in the BIPV when RT-42 is used. This increase is more than double that of the BAPV scenario.
We can conclude that with a low melting temperature the difference between BIPV and BAPV is not significant but becomes important when a higher melting temperature is used and higher temperatures are then preferable.

Table 5. Yearly gain for both BIPV and BAPV.

Type of panel	*BIPV*	*BAPV*
Malaga RT-27 (kWh)	3.52	3.14
Malaga RT-42 (kWh)	5.03	3.75

4.3 *Commercial PCMs and cost analysis*

The Rubitherm RT-27 PCM properties are used in all of the standard model runs. Table 6 shows other commercially available PCMs of which properties have been included in other model runs; results in Table 7. These are all paraffin waxes and share properties in the same range. The difference in energy gain is mainly caused by the melting temperature differences. The theoretical maximum represents an ideal situation in which the PCM has unlimited heat storage capacity, i.e. the capability of keeping the temperature around operating temperature all day.

Table 6. Different commercial PCM properties.

Property	*RT-27*	*RT-42*	*BASF micronal DS 5001*	*Thermusol35*
Melting temperature (^{o}C)	27	42	26	35
Density (kg m^{-3})	880	880	300	780
Heat conductivity (W m^{-1} K^{-1})	0.2	0.2	*n.a.(0.2)*	0.2
Latent heat of fusion (J kg^{-1})	184	174	110	160
Specific heat capacity (J kg^{-1} K^{-1})	2000	2000	*n.a.(2000)*	2500

Table 7. Energy gain for commercial PCMs for Malaga.

Totals (m^{-2} yr^{-1})	*RT-27*	*RT-42*	*BASF micronal*	*Thermusol35*	*Theoretical maximum*
Malaga (10^6 J)	12.7	18.1	8.26	12.4	161
(kWh)	3.53	5.03	2.29	3.44	44.71
(%)	1.56	2.22	1.01	1.52	19.73

In order to see if the option of PCM/PV on a larger scale is possible it is important to look at its economic potential, i.e. will the gained energy efficiency outweigh the cost of the PCM material needed. This results in a simple evaluation of the costs and benefits and it is possible to calculate the payback period for the PCM material using the following formula:

$$PBP(yr) = \frac{pricePCM(€/kg) \cdot Weight(kg/m^2)}{EfficiencyGain(kWh/m^2 yr) \cdot priceElectricity(€/kWh)} \quad (30)$$

The PCM bulk material has to be encapsulated and attached in some form to the back of the PV panel. Additionally there might be fins needed to enhance the conductivity. These additions are assumed to double the price of the bulk material.
The results on payback period are shown in table 8. These show that even with only the bulk material cost taken into consideration the energy gain of the PV/PCM system does not compare to the cost that is paid for the material. The pay back periods are far beyond a considerable limit of 20 years. Only when the temperature is kept around STC conditions all year (theoretical maximum) the payback period is acceptable in the case of Malaga.

Table 8. Cost and payback period of several commercially available PCMs.

	Cost(€/kg) bulk[4]	*Electricity price (€/kWh)*[5]		*Energy gain (kWh yr^{-1} m^{-2})*		*Payback period (yr)*	
		ES	NL	Malaga	Utrecht	Malaga	Utrecht
Rubitherm 27	2.5	0.158	0.185	3.52	2.03	158	234
Rubitherm 42	2.5			5.03	1.88	110	253
Thermusol 35	*n/a* (2.5)			3.44	1.61	161	295
BASF micronal	2.9			2.29	2.23	282	247
Theoretical maximum	2.5			44.71	14.78	12.5	32

[4] Cost prices are deducted from sources [38], [40]
[5] Electricity prices from [37]

5. Discussion

Different PV/PCM systems have been tested by Hasan et al. [10] and it is clear that this combination indeed reduces the temperature of the building integrated PV module and increases its efficiency. Compared to other options of temperature regulation such as forced air circulation design PV/PCM combination brings some positive features such as high heat absorption rate, no moving parts, no electricity consumption and no maintenance cost. Together with the environmentally benign properties of e.g. Rubitherm PCMs this is a promising approach for temperature reduction.
In this research there has been attention paid to the significance of this temperature reduction in terms of energy gain and consequently the cost-effectiveness of such a system.
Although there are a lot of parameters involved in the energy gain calculation and the model is rather simplistic, it is capable of giving a good estimate on the range of yield in energy gain a PV/PCM system can bring. With serious increase in important parameters such as thickness and latent heat of the PCM the results stay in the range of 1-3% of the total yearly energy output.
When taking into account the cost of PCM it turns out the payback periods of a PV/PCM system will be very high which underlines the low economic viability of such an option at the moment. For any further possibilities this means either energy gain has to increase and/or the PCM cost has to go down by 1-2 orders of magnitude.
For a maximum energy gain the important property is the heat storage capacity of the PCM. This includes the latent heat storage, the volume and the density of the PCM. An increase in volume will cause an increase in gain but also in cost. This leaves a possible increase of the latent heat storage as the only option. This is an intrinsic property of the PCM mix and therefore no great increase is expected. The highest latent heat possible at the moment does not reach above 300 kJ/kg [17] and this is not sufficient for a high increase in energy gain as shown by the theoretical maximum that uses a value >1000 kJ/kg.
That leaves the cost of the material that has to decrease. There is no proper data on the price development of PCM material but we can expect the price to slightly go down since PCM has gained attention in the last years as an option in different temperature and energy applications (e.g. PCM wall boards, building climate control, solar energy storage, etc.). For a reasonable payback period under 20 years the price would have to come down to 0.3-0.5 €/kg which is not realistic.
What remains for BIPV is a combination with the inside climate control of the building. There are several methods on the market that use PCMs to keep a controlled inside climate with less energy use (e.g. PCM filled concrete or PCM wallboards). By having the PCM integrated in the roof it controls the temperature of the PV and is also contributing to the inside climate control. This double role in thermal management might still prove a good option for the future. Especially since other options like forced air circulation or hydraulic cooling also require costs for investment and electricity.

6. Conclusion

PCMs have been investigated as a possible option to limit temperature in photovoltaic systems and increase efficiency. There are commercially available paraffin waxes such as Rubitherm 27 that are environmentally friendly and 100% recyclable.
Using properties of these paraffins a simplified heat balance has been used to model the energy output for a yearly period of insolation in both Utrecht and Malaga. The temperature is kept constant at the melting temperature for 2-4 hours a day and this is translated into an energy gain due to the temperature difference and its corresponding increase in PV efficiency.
The uncertainty in the model calculations is significant (e.g. weather conditions, reference efficiency, etc.), as well as the assumptions made in the simplified conduction model. Sensitivity analysis however shows that on average the yield per year of a PV/PCM system is only a small percentage of the yield of the reference case and stays in the range of 1-3%. In a theoretical scenario in which the heat storage capacity has no limit the yield is just under 20%.
The aim of the research was to calculate this yearly yield and also test its economic viability of becoming an option in the BIPV market. When taking into account the cost of electricity and PCM it turns out the extra energy output is too small and the payback period is far above an acceptable 20 years limit. Only the theoretical (but far unrealistic) scenario returns an acceptable payback period of 10-12 years.
This means that the option of PCM as temperature regulation and temperature regulation of PV in general makes no significant impact on the total energy output of a panel. PCM in building integrated PV might be combined with other options such as inside climate control and weather protection in order to be more economically viable.

7. References

[1] Huang, M. (2006). Phase change materials for limiting temperature rise in buidling integrated photovoltaics. *Solar energy 80* , 1121-1130.
[2] Huang, M. (2004). Thermal regulation of building-integrated photovoltaics using phase change materials. *Int. Journal of Heat and Mass Transfer* , 2715-2733.
[3] Huang, M., Eames, P., & Norton, B. (2006). Comparison of a small-scale 3D PCM thermal control model with a validated 2D PCM thermal control model. *Solar Energy Materials & Solar Cells 90* , 1961–1972.
[4] Hasan, A., McCormack, S., 'Huang, M., & Norton, B. (2010). Evaluation of phase change materials for thermal regulation enhancement of building integrated photovoltaics. *Solar Energy*.
[5] Bagnall, D. (2008). Photovoltaic technologies. *Energy Policy 36* , 4390-4396.
[6] Sivanandan, A. (2009). BIPV hotspots in the EU. *renewable energy focus* , 54-55.
[7] Twidell, J., & Weir, T. (2006). *Renewable Energy Resources.* New York: Taylor & Francis.
[8] Iliceto, A., & Vigotti, R. (1998). The largest PV installation in Europe: perspectives of multimegawatt PV. *15 48–53*.
[9] Mei, L., Infield, D., Gottschalg, R., Loveday, D., Davies, D., & Berry, M. (2009). Equilibrium thermal characteristics of a building integrated photovoltaic roof. *Solar Energy 83* , 1893–1901.
[10] Farid, M. M., Khudhair, A., Razack, S., & Al-Hallaj, S. (2004). A review on phase change energy storage: materials and applications. *Energy Conversion and Management 45* , 1597-1615.
[11] Kittel, C., & Kroemer, H. (1980). *Thermal physics.* New York: W.H. Freeman and Company.
[12] Radziemska, E. (2003). Thermal performance of Si and GaAs based solar cells and modules: a review. *Progress in Energy and Combustion Science 29* , 407–424.
[13] Green, M. (1992). *Solar cells.* Kensington: University of New South Wales.
[14] Radziemska, E., & Klugmann, E. (2002). Thermally affected parameters of the current–voltage characteristics of silicon photocell. *Energy Conversion and Management 43* , 1889-1900.
[15] Radziemska, E. (2003). The effect of temperature on the power drop in crystalline solar cells. *Renewable Energy 28* , 1–12.
[16] Zalba, B., Marın, J. M., & Cabeza, L. F. (2003). Review on thermal energy storage with phase change: materials, heat transfer analysis and applications. *Applied Thermal Engineering 23* , 251–283.
[17] Sharma, A., Tyagi, V., Chen, C., & Buddhi, D. (2009). Review on thermal energy storage with phase change materials and applications. *Renewable and Sustainable Energy Reviews 13* , 318–345.
[18] Günther, E., & Hiebler, S. (2009). Enthalpy of phase change materials as a function of temperature: required accuracy and suitable measurement methods. *Int J Thermophys 30* , 1257–1269.
[19] Lamberg, P., Lehtiniemi, R., & Henell, A. (2004). Numerical and experimental investigation of melting and freezing processes in phase change material storage. *International Journal of Thermal Sciences 43* , 277–287.
[20] Jones, A. D., & Underwood, C. P. (2001). A thermal model for photovoltaic systems. *Solar Energy Vol. 70* , 349–359.
[21] Anderson, T., Duke, M., Morrison, G., & Carson, J. (2009). Performance of a building integrated photovoltaic/thermal. *Solar Energy 83* , 445–455.

[22] Jimenez, M., Madsen, H., Bloem, J., & Dammann, B. (2008). Estimation of non-linear continuous time models for the heat exchange dynamics of building integrated photovoltaic modules. *Energy and Buildings 40* , 157–167.
[23] Lamberg, P., & Siren, K. (2003). Approximate analytical model for solidification in a finite PCM storage with internal fins. *Applied Mathematical Modelling 27* , 491–513.
[24] Lamberg, P., & Siren, K. (2003). Analytical model for melting in a semi-infinite PCM storage with an internal fin. *Heat and Mass Transfer 39* , 167–176.
[25] Wang, X., Yap, C., & Mujumdar, A. S. (2008). A parametric study of phase change material (PCM)-based heat sinks. *International Journal of Thermal Sciences 47* , 1055–1068.
[26] Vyshak, N., & Jilani, '. G. (2007). Numerical analysis of latent heat thermal energy storage system. *Energy Conversion and Management 48* , 2161–2168.
[27] (n.d.). Retrieved 2010, from NASA Atmospheric Sciences Data Center. Surface meteorology and Solar Energy: http://eosweb.larc.nasa.gov/sse.
[28] Krauter, S., & Hanitsch, R. (1996). Actual optical and thermal performance of PV-modules. *Solar Energy Materials and Solar Cells 41/42* , 557-574.
[29] Skoplaki, E., & Palyvos, J. (2009). Operating temperature of photovoltaic modules; A survey of pertinent correlations. *Renewable Energy 34* , 23–29.
[30] Zhou, W., Yang, H., & Fang, Z. (2007). A novel model for photovoltaic array performance prediction. *Applied Energy 84* , 1187–1198.
[31] Santbergen, R., & Zolingen, R. v. (2008). The absorption factor of crystalline silicon PV cells: A numerical and experimental study. *Solar Energy Materials & Solar Cells 92* , 432–444.
[32] Jie, J., Hua, Y., Wei, H., Gang, P., Jianping, L., & Bin, J. (2007). Modeling of a novel trombe wall with PV cells. *Building and Environment 42* , 1544–1552.
[33] Bony, J., & Citherlet, S. (2007). Numerical model and experimental validation of heat storage with phase change materials. *Energy and Buildings 39* , 1065–1072.
[34] Chen, C., Guo, H., Liu, Y., Yue, H., & Wang, C. (2008). A new kind of phase change material (PCM) for energy-storing wallboard. *Energy and Buildings 40* , 882–890.
[35] Zukowski, M. (2007). Mathematical modeling and numerical simulation of a short term thermal energy storage system using phase change material for heating applications. *Energy Conversion and Management 48* , 155–165.
[36] (n.d.). Retrieved 2010 from Rubitherm GmbH: http://www.rubitherm.com/
[37] *European Commission*. (n.d.). Retrieved 2010 йил May from http://ec.europa.eu/energy/publications/statistics/doc/2010_energy_transport_figures.pdf
[38] *Deerns.* (n.d.). Retrieved 2010 from http://www.deerns.nl/documents/PCM_Deerns_IBouwman_20081113_v2.0_1.pdf
[39] Farid, M. M., Khudhair, A. M., & Razack, S. (2004). A review on phase change energy storage: materials and applications. *Energy Conversion and Management 45* , 1597–1615.
[40] *Fredrik Setterwall Konsult AB.* (n.d.). Retrieved 2010 йил May from http://www.fskab.com/Annex17/Workshops/EM6%20Arvika/Presentations/Henrik.pdf
[41] *Capzo*. (n.d.). Retrieved 2010 йил May from http://www.capzo.nl/
[42] *Micronal PCM*. (n.d.). Retrieved 2010 from BASF Dispersions & Pigments: http://www.micronal.de/portal/basf/ien/dt.jsp?setCursor=1_290798

8. Appendix

A: Matlab code

```
%FINAL1BIPV

%INITIALIZATION
clear all

Eff = 0.15;       % reference efficiency
a = 0.905;        % absorbance factor (%)
Tm = 315;         % melting temperature PCM (K)
c1 = 500;         % specific heat of glass (J kg^-1 K^-1)
c2 = 2000;        % specific heat of PCM (J kg^-1 K-1)
k  = 0.02;        % thermal conductivity solid  (W m-1 K-1)
x  = 0.04;        % thickness of PCM layer
H  = 184000;      % latent heat of PCM (J kg^-1)
d2 = 880;         % density of PCM (kg m-3)
m1 = 25;          % mass of PV panel without PCM (kg)
m2 = d2*x;        % mass of PCM (kg)
S = 0.04;         % heat absorbance factor
dt = 60;          % time step insolation measurements (s)
d = 0.0065;       % constant for power/temperature relation
K = 10^6;         % constant K/Io (m2 W-1)
Cpv = m1*c1;      % heat capacity for reference PV system  (J K-1)
Cpcm = m2*c2;     % heat capacity for PCM                  (J K-1)
Cff = 1.22;       % fill factor model constant (K m2)
sig = 5.67*10^-8;% Stefan-Boltzmann constant
Es = 0.95;        % emissivity sky , clear sky conditions
Em = 0.90;        % emissivity module
Vm = 2.0;         % average windspeed Malaga
Vu = 3.3;         % average windspeed Utrecht

% DATA (interpolated)
I = load('Utrecht_All_interp1_60sec_I');          % insolation ( W m^-2 )
Tamb = load('Utrecht_All_interp1_60sec_Tamb');    % ambient temperature (K)

n = length(I);

%Initialization & Boundary conditions

Tpv = zeros;   %Tpv is calculated PV temperature with PCM
Tref = zeros;  %Tref is reference PV temperature withouth PCM
Tpv(1) = Tamb(1);
Tref(1) = Tamb(1);

HeatAbsorbed = 0;

%DYNAMIC LOOPS

%PVtemperature with PCM (K)
for i=2:n

    if I(i) ~= 0

    Irr     = I(i)*a;             % (W) irridation
    P       = Cff*((I(i)*log(K*I(i)))/Tpv(i-1));    % (W)  power out
    Ts      = 0.037536*Tamb(i)^1.5+0.32*Tamb(i);
% Sky temperature (K)
    Rad     = sig*Em*(Tpv(i-1)^2-Ts^2)*(Tpv(i-1)+Ts);
```

```
% net radiative heat transfer (W)
    Hfront1 = 1.78*(Tpv(i-1)-Tamb(i))^(1/3);
% Free convection coefficient on front side of panel
    Hfront2 = 2.8+3*Vu;
% wind forced convection coefficient on front side of panel
    Htotal  = (Hfront1^3+Hfront2^3)^(1/3);
% total front convection (W/m2 K)
    Conv    = (Htotal)*(Tpv(i-1)-Tamb(i));
% (W) convection heat transfer

    Conduction1 = k*x*(Tpv(i-1)-Tamb(i));
    Conduction2 = k*x*H*((Tpv(i-1)-Tm));
    Conduction3 = k*x*(Tpv(i-1)-Tamb(i));

         Tpv(i) = Tpv(i-1)+(((Rad+Irr-P-Conv)/Cpv) - Conduction1/Cpcm)*dt;

     if Tpv(i)>= Tm

         Tpv(i)=Tpv(i-1)+(((Rad+Irr-P-Conv)/Cpv) - Conduction2/Cpcm)*dt;
         HeatAbsorbed(i) = k*H*S*(Tpv(i-1)-Tm)*dt;
     end

     if sum(abs(HeatAbsorbed)) >= H*m2 + Cpcm*(Tm-Tamb(i))

       Tpv(i) = Tpv(i-1)+(((Rad+Irr-P-Conv)/Cpv)-Conduction3/Cpcm)*dt;
     end

    else
        Tpv(i) = Tamb(i);
        HeatAbsorbed = HeatAbsorbed*0;
    end
end

%PVtemperature without PCM (K)
for i=2:n
    if I(i)~= 0
        Irr = I(i)*a;
        P   = Cff*((I(i)*log(K*I(i)))/Tref(i-1));
        Ts = 0.037536*Tamb(i)^1.5+0.32*Tamb(i);
        Rad = sig*Em*(Tref(i-1)^2-Ts^2)*(Tref(i-1)+Ts);
        Hfront1 = 1.78*(Tref(i-1)-Tamb(i))^(1/3);
        Hfront2 = 2.8+3*Vu;
        Htotal = (Hfront1^3+Hfront2^3)^(1/3);%;
        Conv = (Htotal)*(Tref(i-1)-Tamb(i));

          Tref(i) = Tref(i-1)+((Rad+Irr-P-Conv)/Cpv)*dt;
    else
        Tref(i)=Tamb(i);
    end
end

TpvC = Tpv-273;
TrefC = Tref-273;

% Temperature difference calculation

Tdiff = Tref-Tpv;
Tdiff2 = Tdiff';
Eref = Eff*a*I*dt; % reference energy output (W)
```

```
Epv  = Eref.*(1+d*Tdiff); % energy output including PCM (W)
Eenhance = Epv-Eref;  % extra energy output per time period due to PCM
total = sum(Penhance) % total extra energy output
```

B. Rubitherm safety data sheet

***RUBITHERM*® RT 27**

Manufacturer/supplier:
Rubitherm Technologies GmbH
Sperenberger Str. 5a, 12277 Berlin
Tel.: +49 30/720004-62, Fax: +49 30/720004-99

2. Potential hazards

EEC-labelling: Xn, harmful

Potential dangers to health and environment:
In case of swallowing product lung damage can be caused.

Danger of fire and explosion:
Low risk. Product creates only ignitable mixtures or burns, if
temperature exceeds flash point.

3. Composition/information of ingredients

Chemical characterisation:
Solid saturated hydrocarbons,
molecular formula C_nH_{2n+2}

CAS-No: 64771-72-8

EINECS-No: 265-233-4

4. First-aid measures

Inhalation:
Take concerned person to fresh air. In case of lasting aches and
pains take medical advices.

Eye contact:
In case of eyes contact rinse out eyes. In case of irritation take
medical advices.

Skin contact:
In case of skin contact wash concerned area with water and soap.
In case of irritation take medical advices. Contact with liquid
product skin burns can be caused. Cooling burned skin and take
medical advices.

In case of swallowing:
Drink water and rinse out mouth. Don't induce vomiting, risk of
aspiration. Take medical advices immediately.

5. Fire-fighting measures

Suitable means for extinguishing:
Carbon dioxide, foam, powder, sand, water mist

Unsuitable means for extinguishing:
water jet

Special hazards caused by the substance, its combustion products or arising gases:
Product fumes and air can cause explosive conglomerates
heavier than air. Inflammation by hot surfaces, unshielded
flames and sparks.
Don't inhale combustion gases and suspended matter which
formed at combustion. Carbon monoxide, carbon dioxide and

6. Measures in case of unintended release

Personal precautions:
Caution of wet floor by leaking product. Slip hazard.
Avoid inhalation of product fumes. Keep product away from ignition
sources, don't smoke.

Environmental precautions:
It's not allowed to drain into environment, into bodies of water or
savage system.
Avoid soil contamination.

Methods for cleaning:
Solid: remove product mechanically
Liquid: use binder to bind liquid product, than remove it mechanically.

7. Handling and storage

Handling

Advices for safe handling:
No special measures necessary while using correctly.
Avoid skin- and eyescontact.

Advices for protection against fire and explosion:
Product mist and air can cause explosive conglomerate.

Storage

Requirements for storerooms and containers:
Store the product cool, dry and in closed barrels devoid of light. Avoid
storage nearby from ignition or heat sources.
Take measure against electrostatic charging. Earth appliances.
Store liquid product in heatable tanks. Avoid the formation of aerosols
and product mist at the decant.

Information for storage together with other products:
Avoid storage together with strong oxidising agents.

8. Exposure controls / personal protection
Ingredients with occupational exposure limits which should be monitored:

1. Germany/Switzerland/Austria
There is no AGW-value for paraffin wax.

2. Germany:
For aerosols and fine dust AGW-value of 3 mg/m³ has to
be kept to.

3. USA
TLV-value for paraffin vapour: 2 mg/m³

Technical measures of control and air ventilation
Ensure good ventilation at workplace in case of handling the product in
closed rooms with higher temperature. Product concentration is to be
kept under exposition threshold values.

Personal protective equipment:
Hand protection: protective gloves made of rubber
Eye protection: safety goggles
Body protection: protective clothes
Breathing protection: In case of arising gases and inadequately
ventilation at workplace use breath apparatus.

soot can also develop.
Special protective equipment in closed rooms:
Use breathing apparatus independent from ambient air.
Additional information:
Cool endangered containers externally with water
Fire class according to DIN-EN 2: B

9. Physical and chemical properties
Physical state: at room temperature
solid
Colour: clear (liquid), whitish
(solid)
Odour: odourless
pH-value at 20°C: n.e.
Melting point (OECD 103): 25 - 28°C
Typical: 27°C
Boiling range (OECD 103): 300 - 330°C
Flash point: approx. 164°C
Auto flammability: > 220°C
Explosive limit in air: 0.3 - 5Vol.-%
Vapour pressure at 50°C (OECD104): 0.048 kPa
Vapour density: 9
Density at 40°C (DIN 51 757): 0.756 g/ml
Solubility at 20°C - in water: < 0.0022 mg/l
Viscosity at 50°C (Brookfield): 26.32 mm²7s
n.a. = not applicable; n.e. = not established
10. Stability / reactivity
Conditions to avoid:
No hazard reactions under normal conditions.
Avoid high thermal load.
Material to avoid:
Strong oxidising agents.
Decomposition products:
None.
11. Toxicological information
Acute toxicity :
Orale LD50: > 5000 mg/kg (Rat)
Dermale LD50: >2000 mg/kg (Rat)
Chronically toxicity: LOEL = 9600 mg/kg (skin, mouse,
140 days) (C14)
Skin irritation: slightly irritant
Eye irritation: slightly irritant
Sensitisation: not available
Mutagenic: not mutagenic
Carcinogenic: not carcinogen
12. Environmental details
Avoid drain into environment.
Elimination/persistence and degradability:
Easy biological degradable (OECD 301 F).
Aquatic toxicity:
LC50 / fish: no reaction
EC50 / daphnia (2 days): no reaction
EC50 / algae (3 days): no reaction

13. Disposal considerations
After reprocessing, the product can get used again or utilised thermally,
otherwise it can be disposed off after consulting with authorities
according to the following waste disposal codes (European Waste
Catalogue):
EWC-Code Description
07 01 04 other organic solvent washing liquids and
mother liquors
07 01 99 wastes not otherwise specified
Packaging:
Drums: can be returned to supplier or producer
14. Transport information
Product is not a hazardous good according to ADR/RID;
GGVs/GGVE, ADNR/ADN; IMDG/GGVSee; ICAO-TI
and IATA-DGR).
No dangerous good.
15. Statutory provisions
Labelling in accordance with the EEC directives:
Xn harmful
Risk-phrase, R-phrase:
R 65 Harmful. In case of swallowing product lung
damage can be caused.
Safety advice, S-phrase:
S 2 keep away from children
S 23 Do not inhale gas/smoke/fumes/aerosol
S 24 Avoid contact with skin
S 62 In case of swallowed, do not induce vomiting!
Take medical advice and show packaging and label.
Classification according to VbF: Not applicable
TA-Luft: Substance class 3.1.7.III
Waterhazard class (WGK): 1
StörfallVo: Not applicable
Swiss: BAG-T-Nr.610200;
Poison class: 0
16. Other information
Literature:
Ullmanns Encyclopädie der technischen Chemie
4. Auflage, Band 24, Kapitel "Wachse aus Erdöl",
Verlag Chemie GmbH, 1983.
This safety data sheet contains only safety related information.
For specific data see product data sheet.
The information on this data sheet is gathered to the best of RUBITHERMS
knowledge and belief and fits as the experience stand at the moment.
RUBITHERM doesn't guarantee the adherence of certain features in sense
of legally binding.
In case of questions please call number given in point 1.

Rubitherm-Technologies GmbH